



Light-curve Recovery with the Vera Rubin Observatory's LSST. I. Pulsating Stars in Local Group Dwarf Galaxies

M. Di Criscienzo¹, S. Leccia², V. Braga¹, I. Musella², G. Bono³, M. Dall'Ora², G. Fiorentino¹, M. Marconi², R. Molinaro², V. Ripepi², K. Carrell⁴, Y. Choi⁴, S. Savarese², and L. Schreiber⁵

¹ INAF-Osservatorio Astronomico di Roma, via Frascati 33, I-00078, Monteporzio Catone, Roma, Italy; marcella.dicriscienzo@inaf.it

² INAF-Osservatorio Astronomico di Capodimonte, Salita Moiariello, 16, I-80131 Napoli NA, Italy

³ Università degli studi di Roma Torvergata, Macroarea di Scienze M.F.N., Via della Ricerca Scientifica, 1, I-00133 Roma, Italy

⁴ Angelo State University, 2601 W Avenue N, San Angelo, TX 76909, USA

⁵ INAF-Osservatorio di Astrofisica e Scienza dello Spazio Bologna, Via Piero Gobetti, 93/3, I-40129 Bologna, Italy

Received 2022 December 9; revised 2023 January 30; accepted 2023 January 31; published 2023 March 16

Abstract

This investigation is mainly focused on the LSST Survey Strategy Optimization process, a bottom-up approach that turned out to be quite effective in involving the scientific community in the definition of the LSST observing strategy. We are mainly interested in using radial variables (RR Lyrae, classical Cepheids, long-period variables) as stellar tracers and distance indicators, and we developed a new tool called `PulsationStarRecovery` to quantify the recovery of the light-curve period and amplitude from an LSST-simulated time series. The outputs of this code are pulsation parameters (period, amplitude, mean magnitude) together with quantitative information concerning the difference between the shape of the light curve and template light curves. Furthermore, we apply the newborn metric to simulate LSST observations and recovery of different types of pulsating stars hosted by selected massive stellar systems (19 Local Group dwarf galaxies and the Large Magellanic Cloud) to show how the recovery changes according to distance and variable-star type. We show that this exercise is essential to understand the potential of LSST in this field since excellent recovery is necessary to optimize the use of predicted period–luminosity, period–amplitude, and color–color relations to constrain the cosmic distance scale and the metallicity distribution function of different stellar populations.

Unified Astronomy Thesaurus concepts: [Surveys \(1671\)](#); [Pulsating variable stars \(1307\)](#); [Dwarf galaxies \(416\)](#); [Light curve classification \(1954\)](#)

1. Introduction

Vera Rubin Observatory's Legacy Survey of Space and Time (LSST) will deliver in the next decade a 500 PB set of images and data products addressing some of the most pressing questions about our Galaxy and Local Group (LG) galaxies (Ivezic et al. 2019). LSST will detect millions of variable stars, providing an impressive database of stellar pulsators such as RR Lyrae (RRL), Cepheids, and long-period variables (LPVs) hosted in different Galactic and extragalactic environments characterized by different chemical compositions and star formation histories (halo, bulge, globular clusters, LG dwarf galaxies). The expected duration of the survey is 10 yr, and it will be performed in six different photometric bands. LSST will allow us, for the first time, to investigate stellar variability regardless of the pulsation period, including secondary modulations characterized by longer time-scales such as the occurrence of the Blazhko phenomenon in RRLs or the secondary periodicity in LPVs.

LSST will bring forward several indisputable advantages:

1. to constrain on a quantitative basis the accuracy of the different groups of variable stars as distance indicators and to investigate the impact that the environment (metallicity) has on their properties;
2. to use relative distances to trace for the first time the 3D structure associated with old (RRLs), intermediate

(LPVs), and young (classical Cepheids, CCs) stellar tracers;

3. to identify extended halos, stellar streams, and possible overdensities around nearby stellar systems, thus providing solid constraints on the early formation and evolution of the Galactic spheroid;
4. the large and homogeneous samples of variable stars will allow us to validate physical and numerical assumptions adopted to constrain evolutionary and pulsation models;
5. together with Gaia and ongoing large spectroscopic surveys, the Vera Rubin Observatory's LSST will provide a unique opportunity to investigate the role that chemical composition plays in the cosmic distance scale (primary and secondary distance indicators).

These are just some of the scientific cases that will greatly benefit from LSST.

The commissioning of the Vera Rubin Observatory's telescope was planned in less than 2 yr and the scientific community has been involved through Science Collaborations (SCs) in setting and refining the observing strategy. In particular, the Vera Rubin Observatory has involved the scientific community in setting and refining the details of the observing cadence. The reader interested in a more detailed discussion concerning the role played by the Transient and Variable Stars (TVS) SC in the decision-making process to optimize the observing strategy is referred to Bianco et al. (2022).

In this context, we investigated different groups of variable stars characterized by different light-curve shapes, periods, absolute mean magnitudes, and luminosity amplitudes. In



Original content from this work may be used under the terms of the [Creative Commons Attribution 4.0 licence](#). Any further distribution of this work must maintain attribution to the author(s) and the title of the work, journal citation and DOI.

Table 1
Templates' Type, Periods, Mean Magnitudes, and Amplitudes in the Six Rubin Photometric Bands

| Type | $P(\text{days})$ | $\langle Mu \rangle$ | Au | $\langle Mg \rangle$ | Ag | $\langle Mr \rangle$ | Ar | $\langle Mi \rangle$ | Ai | $\langle Mz \rangle$ | Az | $\langle My \rangle$ | Ay |
|------|------------------|----------------------|-------|----------------------|-------|----------------------|--------|----------------------|-------|----------------------|-------|----------------------|-------|
| RRab | 0.605 | 1.508 | 0.999 | 0.529 | 1.105 | 0.395 | 0.849 | 0.390 | 0.690 | 0.421 | 0.614 | 0.424 | 0.615 |
| RRc | 0.383 | 1.474 | 0.617 | 0.482 | 0.694 | 0.400 | 0.528 | 0.431 | 0.426 | 0.483 | 0.380 | 0.489 | 0.382 |
| CEP1 | 0.979 | 0.254 | 0.700 | -1.036 | 0.580 | -1.315 | 0.4038 | -1.347 | 0.332 | -1.319 | 0.298 | -1.318 | 0.292 |
| CEP2 | 10.750 | -2.042 | 2.224 | -3.816 | 1.432 | -4.370 | 0.963 | -4.516 | 0.779 | -4.558 | 0.683 | -4.583 | 0.649 |
| LPV | 349.207 | -0.342 | 5.843 | -3.843 | 7.203 | -5.21 | 6.784 | -5.919 | 4.021 | -6.310 | 3.001 | -6.582 | 2.151 |

particular, we focused our attention on RRLs and CCs located inside the so-called Cepheid instability strip and LPVs located inside the Mira instability strip. To accomplish this goal, we developed a new tool (metric), which, starting from a variable-star template, generates the time series based on a given LSST cadence, recovers its pulsation period, and performs a multiband fit of the simulated light curves and estimates mean magnitudes and amplitudes in the six Rubin photometric bands *ugrizy*.

The main aim of this investigation is to make available to the LSST Survey Cadence Optimization Committee (SCOC), and to the entire community interested in variable stars, a solid and easy-to-use tool to investigate in detail the impact that LSST observing strategies have on the identification and characterization of variable stars. According to the SCOC, the chosen observational approach will not be written “in stone”; therefore, the tool we developed can be also used during the survey to propose a change in the LSST cadence that can allow us to accomplish relevant and compelling scientific results not only within the TVS community but also in the Stars, Milky Way and Local Volume Science Collaboration (SMWLVC) community. Moreover, the current metric can also be adopted by the TVS community to define new scientific cases not yet covered in the TVS road map (Hambleton et al. 2022).

The structure of the paper is as follows. In Section 1 we describe in detail the metric `PulsatingStarRecovery`. The following two sections are focused on different classes of pulsating stars in selected LG environments, and our new tool is used to analyze different proposed observational strategies. Our conclusions close the paper.

2. PulsatingStarRecovery: A New Metric

The Metric Analysis Framework (MAF; Jones et al. 2020)⁶ already provides valuable and straightforward metrics to quickly analyze light curves such as `TransientMetric`. However, we deemed it essential to build a new one to forecast the actual scientific performance of a proposed cadence, using adequate templates and the best possible methodology.

`PulsatingStarRecovery` metric is a sophisticated expert metric built to understand the influence of a given LSST survey strategy on the recovery of the period and shape of the light curve of pulsating stars at a given distance and a given point of the sky. It is divided into three main parts, each dealing with a specific task (see Figure 1). The first, called `LcConstructor`, builds the temporal series of a pulsating star at a given position in the 3D sky, starting from a theoretical light curve (template with specific pulsation properties) and a given LSST survey cadence strategy and then performing a quick analysis of the light-curve sampling. The second part (`LcPeriod`) computes the periodogram of the simulated

temporal series and derives the best period through a multiband analysis performed with the `Gatspy` software (VanderPlas & Ivezić 2015). The third and final part of the metric, called `LcFitting`, computes the models that best fit the simulated light curves (simulated temporal series + best period) separately in each band. This step is essential to derive recovered amplitudes and mean magnitudes. As a result, `PulsatingStarRecovery` returns a complete dictionary that contains a large number of quantities useful to test the recovery of that particular light curve.

In the following subsection, we describe each of these steps in detail.

2.1. LcConstructor: From a Theoretical Model to the Simulated Temporal Series

The starting point of our metric is a nonlinear convective 1D hydrodynamical model of pulsating stars. For RR Lyrae and CCs, we have used selected pulsation models computed by Marconi et al. (2015) and De Somma et al. (2020), while the LPV template is computed by Trabucchi et al. (2021). The theoretical bolometric light curves have been transformed into the Rubin *ugrizy* bands by using the bolometric corrections tables provided by Chen et al. (2019). Table 1 gives the pulsation properties of the templates used in this paper.

The function `LcConstructor` derives the temporal series for each template using the survey cadence strategy described by a given `OpSim`⁷ output at a given point of the sky. For each LSST *ugrizy* band, the numbers of visits are derived, and for each visit, valuable information is stored, such as the 5σ depth (m5) useful to retrieve the signal-to-noise ratio (S/N)⁸ and photometric errors, the sky brightness (`skyBrightness`) and the effective FWHM (`seeingFwhmEff`) to compute the saturation limit.⁹ Figure 2 shows the simulated light curves obtained after 1 yr of survey, when our templates are positioned at the Sagittarius dwarf galaxy distance and position (R. A. = 283.76292, decl. = 30.47833, $d = 0.02$ Mpc), and when the survey cadence is described by `baseline_v2.0_10yrs` (for details on this particular simulation, see Bianco et al. 2022).

Each point (corresponding to a single visit) in Figure 2 is not exactly on the displayed theoretical curve from which it was extracted because the simulated photometric error derived from

⁷ The Operations Simulator (OpSim) is an application that simulates the field selection and image acquisition process of the LSST over the 10 yr life of the planned survey (Delgado & Reuter 2016; Reuter 2016). Each run produces an SQLite database of visits with data describing each visit (e.g., the start time, filter used, simulated seeing, etc.).

⁸ Using MAF's basic metric `retrieveSnR`.

⁹ In our analysis the saturation limit is computed with `SaturationStacker`: https://rubin-sim.lsst.io/api/rubin_sim.maf.stackers.BaseStacker.html.

⁶ <https://rubin-sim.lsst.io/>

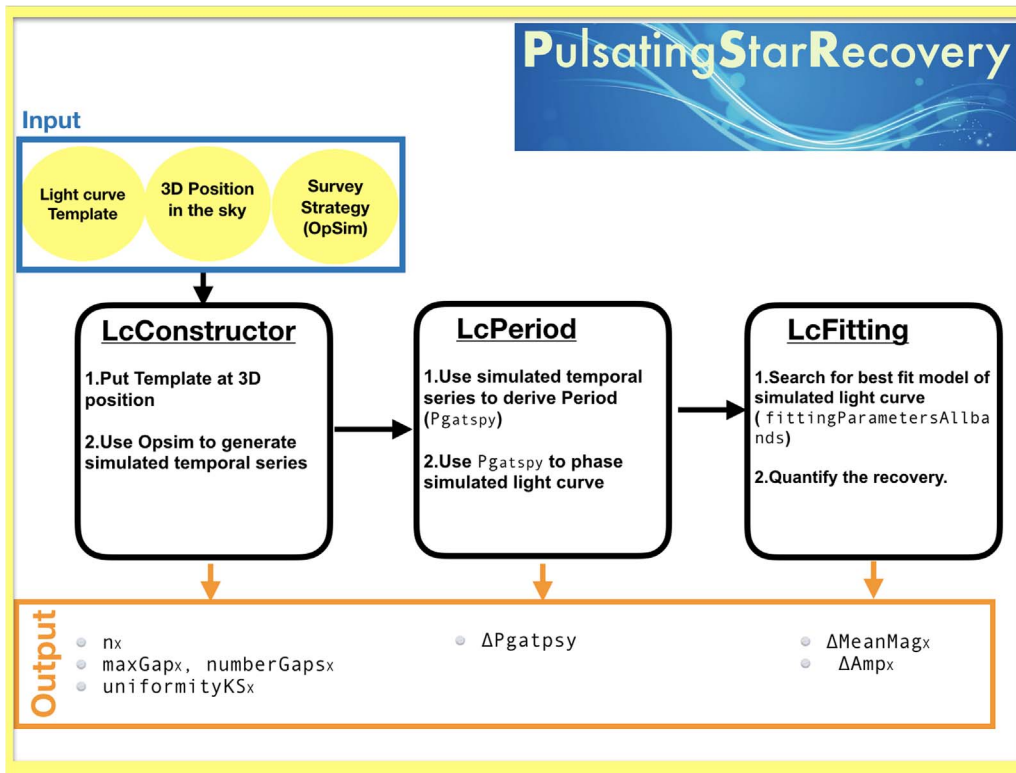


Figure 1. Software scheme diagram. Output quantities are described in Section 2.4 and Table 2.

OpSim for each visit has been added to the magnitude. In this particular case, these errors are very small (less than a thousandth of a magnitude for most of the visits) due to the proximity of Sagittarius.

LcConstructor computes significant quantities at this stage, such as the number of not-saturated visits (n_x , where X is the filter) and a few numbers that quantify the simulated light-curve sampling. In particular, it computes the phase difference between the two most distant consecutive phase points ($maxGap_x$), the number of large gaps ($numberGaps_x$) where large means $>0.7 * maxGap_x$, and $uniformityKS_x$ is a modified version of the result of `UniformityMetric` by Peter Yoachim¹⁰ that uses the Kolmogorov–Smirnov test to compute how uniformly the observations are spaced in phase (and not in time as the original metric does). $uniformityKS_x$ is a value between 0 (uniform sampling) and 1.

2.2. LcPeriod: Period Extraction

To extract the period from the simulated temporal series, the `PulsatingStarRecovery` metric uses `Gatspy`, an open-source, Python-based tool to study the astronomical time series (VanderPlas 2015). In particular, we used its `MultibandLombscargle` option,¹¹ which implements the flexible multiband model described in VanderPlas & Ivezić (2015). Using simulated light curves and randomly subsampled SDSS Stripe 82 data, the authors have demonstrated the superiority of this method in deriving the period, compared to other methods from the literature.

¹⁰ https://rubin-sim.lsst.io/api/rubin_sim.maf.metrics.UniformityMetric.html

¹¹ In particular we choose the option $(Nbase, Nband) = (1, 0)$, which is called the shared-phase model. In the shared-phase model, all variability is assumed to be shared between the bands, with only the fixed offset between them allowed to float (see VanderPlas & Ivezić 2015 for a more detailed explanation).

Figure 3 shows on the left simulated *ugrizy* observations of the RRC in Sagittarius after 1 yr of observations, which translate, according to the chosen `OpSim` into 5, 8, 18, 20, 15, and 20 not-saturated observations in the *ugrizy* filters, respectively. No single band has enough information to detect the period, as shown in the left upper panel, where the periodogram is computed separately for all the filters. On the contrary, the shared-phase multiband approach (lower-right panel), combining the information from all six bands, results in a significant detection of the actual period as demonstrated by the labeled small value of the difference between the derived and template’s period (ΔP_{gatspy}). The result is even more significant ($\Delta P_{gatspy} = 0.000008$), doubling the number of years. Unfortunately, the author is no longer supporting `Gatspy`, so the TVS SC has proposed replacing it with a modern and well-maintained code that would benefit a lot of TVS science. ‘‘NewGatspy’’ was suggested as a development project for the General Pool of software development effort from the International In-Kind process and will be inserted in our metric as soon as the new software is available.¹²

2.3. Lcfitting: Fit of the Simulated Light Curve

Once we obtain the period we use it to phase the simulated time series and in the last part of the metric, called `Lcfitting`, we perform the fit of the simulated light curves.

We have decided not to use `Gatspy` at this point. First, because we are not sure that this software will continue to survive in its current form but above all, because contrary to what we did to derive the period here, we want to treat all bands individually as light curves change significantly from the

¹² Moreover, the referee pointed out that there is some work going on through LINCC (<https://www.lsstcorporation.org/linc/>) to incorporate `Gatspy` into astrology.

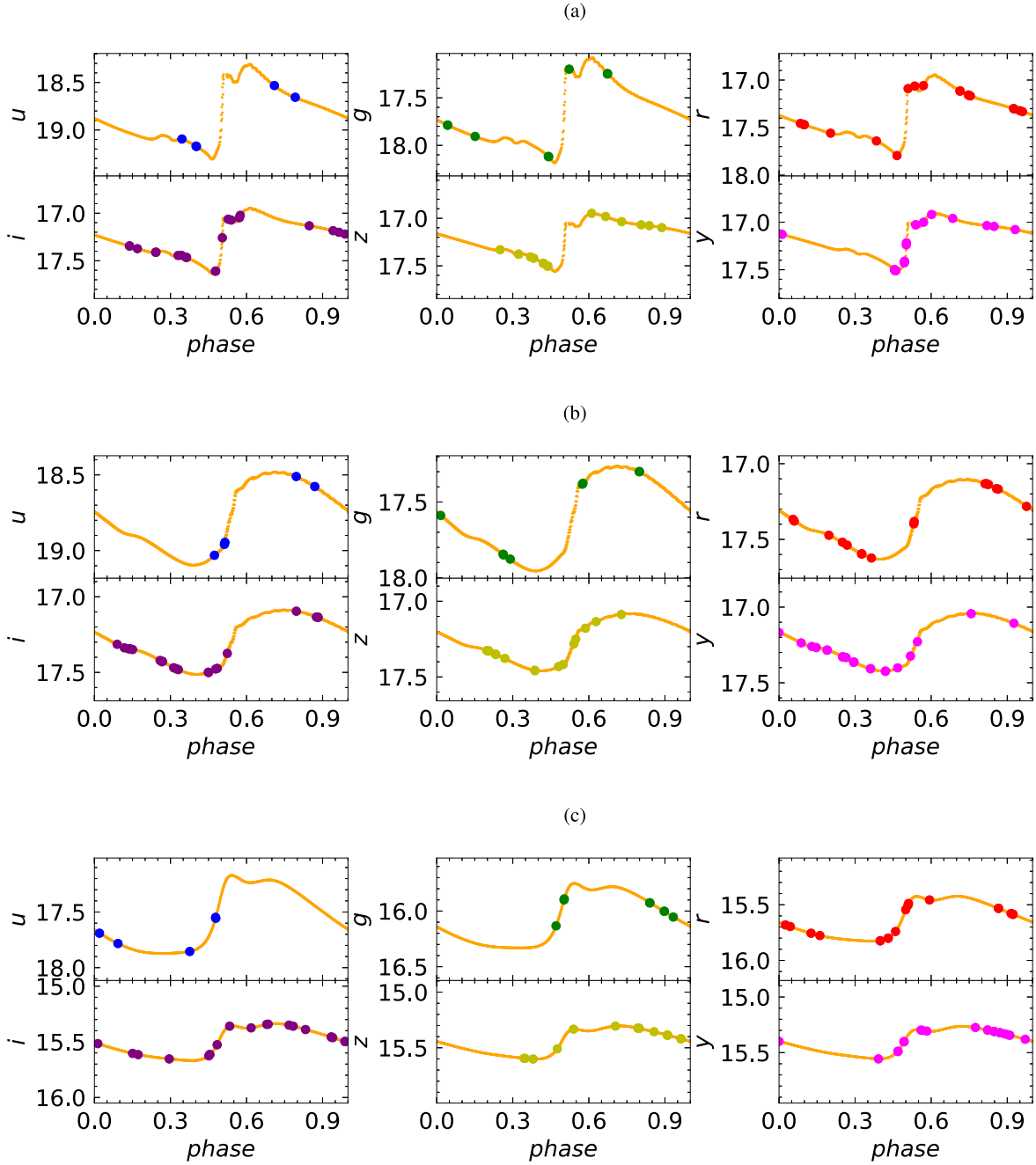


Figure 2. Template’s light curves (orange) and simulated observations (colored points, crossed are used for saturated magnitudes) in *ugrizy* of selected RRAb (a), RRC (b), short-period CCs CEP1 (c), long-period CCs CEP2 (d), and LPVs (e) at the position and distance of the Sagittarius dwarf galaxy (R.A. = 283.76292, decl. = -30.47833 , dist = 0.02). The survey cadence is simulated by `baselinev2.010 yrs.db`, and only the observations expected in the first survey’s year were taken into consideration. Photometric errors (<0.001 mag) derived from Opsim and used in the simulation (see text) are too small to be shown.

u to the y band, not only in amplitude but also in shape. The light curve is modeled with a truncated Fourier series:

$$\text{mag}(t_j) = zp + \sum_i A_i \sin(i * 2\pi\nu_{\max} t_j + \phi_i), \quad (1)$$

where t_j is the epoch of the j th measurement, A_i and ϕ_i are the amplitude and phase of the i th harmonic, ν_{\max} is the frequency with maximum power in the frequencygram. Zero-point (zp), period ($1/\nu_{\max}$), amplitudes (A_i), and phases (ϕ_i) of the harmonics are determined using the Levenberg–Marquardt nonlinear fitting algorithm. As trial values for zero-points and periods, the average

mean magnitude from the model and the period from the `Gatspy` best period are given. The number of harmonics (`numberOfHarmonics`) is fixed, and it is an input parameter that depends on the variable-star type and sampling. We chose a small number (2–3) of harmonics for simple quite-sinusoidal light curves, while a bigger one (6–7) is needed for more complex (and well-sampled) shapes to have a good fit. In case of poor sampling of the light curve, we suggest using a low number of harmonics to avoid spurious oscillations. For example, an inspection of Figure 4, where the simulated RRC light curve in Sagittarius is

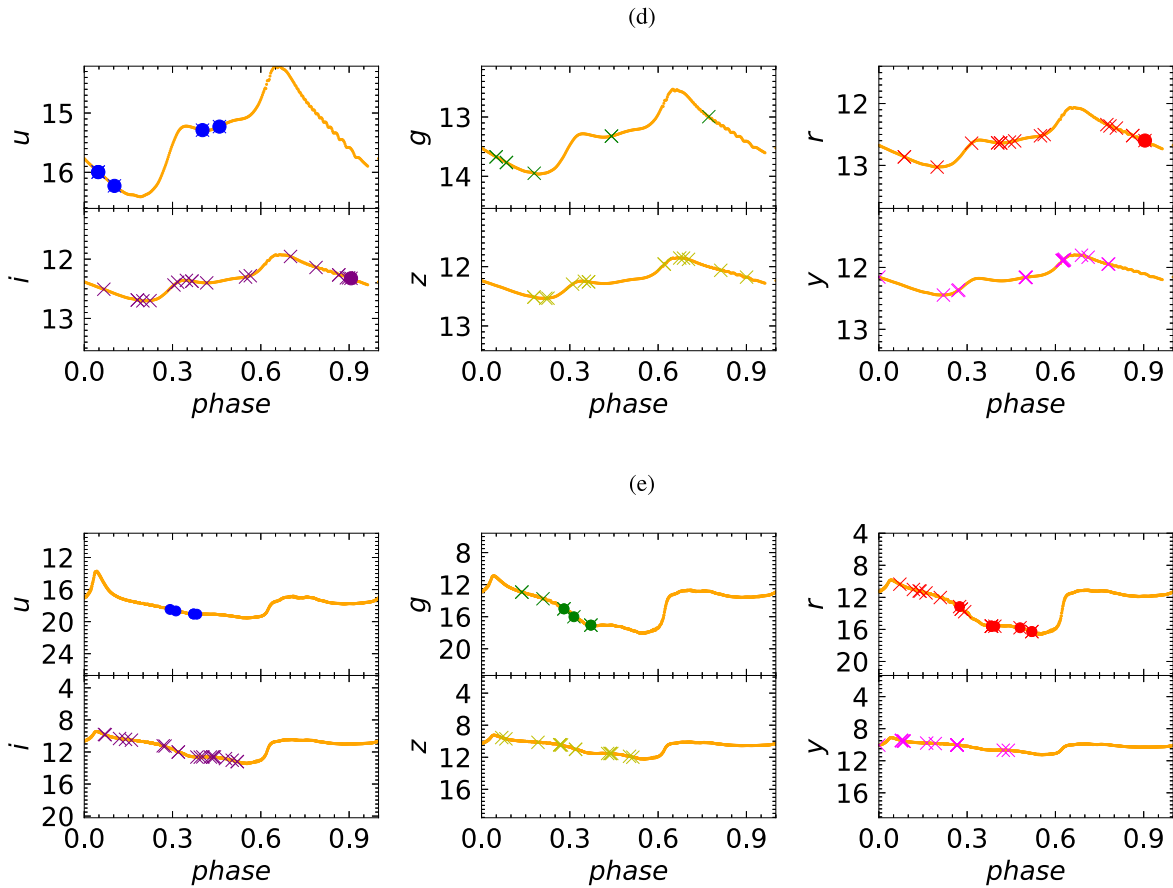


Figure 2 (Continued.)

shown together with the result of the fitting procedure using `numberOfHarmonics = 3` for all the photometrical bands, suggests that this choice for the number of harmonics is a good compromise for the *r*, *i*, and *y* bands but it is too high for *z* due to the large gap in phase. In the case of *u* and *g*, the number of visits is too low to perform the fit, and for this reason, only the points of the simulated light curves are shown.

It is important to stress that the light-curve fit is crucial as it gives valuable information to fully characterize a pulsation star and eventually classify it. For example, the period–amplitude Bailey diagram (Bailey 1902) is the first example of a tool to distinguish between RRab and RRC pulsation modes. In this diagram, the two subclasses occupy well-separated loci, allowing us to classify the stars. Notice that the peak-to-peak amplitude can be measured only from the fitted model of the light curve. Adopting the results of the nonlinear Fourier modeling amplitude ratios and phase differences ($R_{ij} = A_i/A_j$; $\phi_{ij} = \phi_i - i \times \phi_j$) can be computed for the light curve.

These parameters are usually known as the Fourier decomposition parameters (Simon & Lee 1981). The position of the star in the period– R_{12} , period– ϕ_{21} , and R_{12} – ϕ_{12} planes can help to distinguish between the RRC and RRab pulsation modes.

The shape of the light curve is also linked to intrinsic quantities such as metallicity. The metallicity ($[Fe/H]$) of single-mode RR Lyrae stars with errors of the order of 0.3 dex can be inferred from the ϕ_{31} Fourier parameter of the light curve, provided that the light curve of the RRab

pulsators satisfy “regularity conditions” defined by Jurcsik & Kovacs (1996), Cacciari et al. (2005), and Nemeč et al. (2013) for RRC.

2.4. Metric Outputs

The `PulsationStarRecovery` metric, after performing the steps described in the previous sections, returns a complete dictionary containing a selection of useful quantities calculated in each step. Table 2 gives a brief description of all the quantities contained in the dictionary. They are organized into three groups mirroring the three different steps carried out by our metric and described in the last subsections. We also give two quantities essential to evaluate how good our light-curve recoveries have been: $\Delta\text{MeanMag}_X$, obtained by subtracting fitted light curves and templates’ mean magnitude, and ΔAmp_X , the difference between the peak-to-peak amplitude (Amp_X) and the theoretical amplitude of the light curve. We have chosen not to define an a priori threshold for the recovery because this depends on the scientific case.

In Table 3, we show how these two differences change as a function of observation years and the number of visits in filters *g* and *r* in the case of the RRC template located in Sagittarius. It is worth noting that after 1 yr of observations in *r* (but the same is valid for all the most populous bands *izy*), the adopted fitting technique would deliver mean magnitudes and amplitudes differing from the true ones by a few thousandths of magnitudes. Instead, since the number of visits at a given survey’s year is much lower in optical bands, this precision, in *g* for example, is obtained after more years.

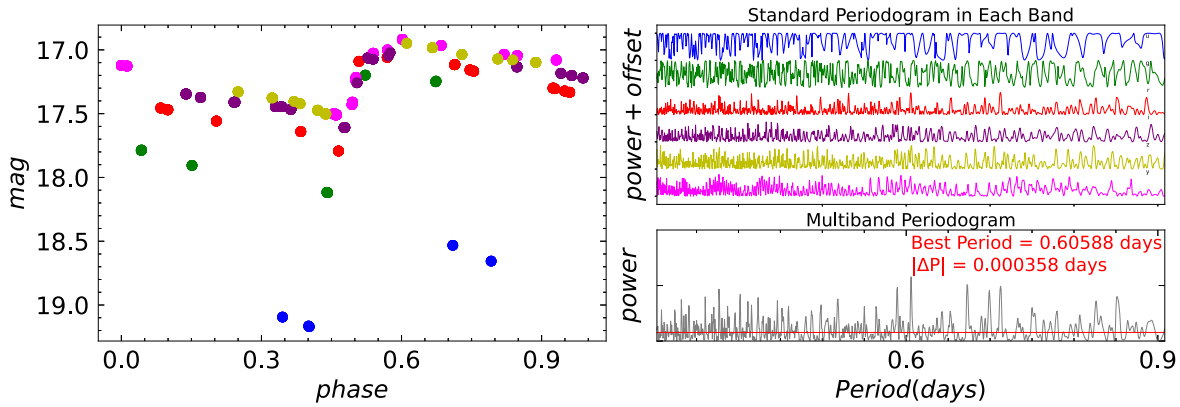


Figure 3. Left: simulated *ugrizy* observations of a typical RRab in Sagittarius as in Figure 2. Right: single periodogram in each band (up) vs. multiband periodogram computed with a shared-phase ($N_{\text{base}}, N_{\text{band}} = (1, 0)$) multiband (down). The last approach fits a single model to the full data and clearly recovers the true period ($P = 0.38354$ days).

2.5. Metric History

We emphasize that we started building this metric for the 2018 Call for Survey Strategy (Clementini et al. 2018) and later refined it for the Cadence Note 2021 (Musella et al. 2021). Thanks to the Rubin community’s input, our metric has been further modified and simplified. In the last months, in particular, `PulsatingStarMetryic` has undergone a long process of revision under the supervision of Lynne Jones.¹³ Thanks to this upgrade, `PulsatingStarMetryic` works like any MAF metric, and anyone can execute it using a single execution of the the Operation Simulator (`Opsim`) and a slicer.¹⁴ The latest version of the metric is loaded on GitHub and can be found at https://github.com/MARCELLADC/rubin_sim/blob/main/rubin_sim/maf/mafContrib/PulsatingStarRecovery_MAF.py.¹⁵ The result will be a dictionary that contains, for each of the selected points of the sky, the quantities described in Table 2.

3. A Test Case: Pulsating Stars in Local Group Dwarf Galaxies

To prove our new metric potential, we first studied the recovery of pulsating variable stars’ light curves in a selected sample of LG galaxies. In recent work (Marconi et al. 2022), we have shown that the application of the period–luminosity–metallicity (PLZ) and period–Wesenheit–metallicity (PWZ) relations to future Rubin LSST observations of RR Lyrae in a massive stellar system will represent a powerful tool to derive mean and individual distances. To make these relations useful, the mean magnitudes that we include must be recovered with an accuracy comparable to or better than the rms of the relations (around 0.1; see column 5 of their Table 5). This section will show how this accuracy changes with the distance and type of pulsating variable and whether this depends on the adopted LSST cadence strategy.

On the other hand, these relations can be used to derive the metallicity distribution of the investigated sample of pulsating

stars, which is crucial to derive the chemical enrichment of the parent galaxy. Marconi et al. (2022) have also shown the value of exploring the color–color diagram constructed from the intensity-weighted mean magnitudes as a diagnostic tool to constrain the metallicity. The highest sensitivity to metallicity is revealed in the $g-r$ versus $u-g$ plane, while the $r-i$ versus $g-r$ diagram shows the best-defined relations. The latter has the advantage of producing well-separated (in metallicity) linear distributions, with slopes that are similar to each other and consistent with the reddening vector one. This occurrence implies that the relation between observed $r-i$ and $g-r$ is not expected to be significantly affected by uncertainties in reddening corrections and can be helpful in systems affected by differential reddening.

To select the environments where we run tests, we started from the Karachentsev et al. (2013) catalog of galaxies and selected those within the LG (~ 1.5 Mpc) and with decl. $< 13^\circ$ since we are interested in the main LSST survey. To include in our sample only dwarf galaxies, we have selected all the galaxies smaller than the Magellanic Clouds (MCs) ($M_* < 0.5 \times 10^9 M_\odot$, where M_* is the stellar mass) and with $M_* > 1 \times 10^6 M_\odot$ to remove ultrafaint galaxies. The MCs, only recently included in the main survey WDF, deserve a separate discussion and will be addressed in detail in the next section. Table 4 shows the result of our selection, including the galaxies arranged by distance. Figure 5 depicts the selected galaxies in an Aitoff diagram colored according to their distance.

In Figure 6, we included the average apparent magnitude of our RRab’s template in each selected galaxy plotted against the detection limit. In those galaxies above the bisector (starting from the top, Sagittarius, Sculptor, Sextans, Carina, and Fornax, respectively), stars with a magnitude equal to our template’s average magnitude are observable in all filters as they are more luminous than the limiting magnitude derived by `Opsim`.¹⁶ From Figure 6, we deduce that, if considered as static stars with magnitude equal to the RRab template intensity-weighted mean magnitude, our template can be observed up to Leo I at 0.26 Mpc (cross) in at least two filters (g and r). The same applies to the RRc, which have similar mean absolute magnitudes, while stars with a magnitude equal to the average magnitude of CEP1 and CEP2, being brighter, can also be observed in more distant galaxies of the sample, and in particular up to NGC 6822 and Sex A, respectively.

¹³ LSST Performance Scientist working on the optimization of the LSST survey strategy.

¹⁴ In this context, we would like to mention the important contribution of the two co-authors from Angelo University who, within the Kickstarter Programme “Building a Diverse Generation of Rubin Scientists,” have tested the metric giving back important feedback.

¹⁵ To see an example of its use at a given 3D position in the sky, please look at this notebook: https://github.com/MARCELLADC/rubin_sim_notebooks/blob/main/maf/science/PulsatingStarRecoveryNotebook_MAF.ipynb.

¹⁶ The limiting magnitude for each galaxy was obtained by averaging all the visits since it depends on the seeing, which can vary from visit to visit.

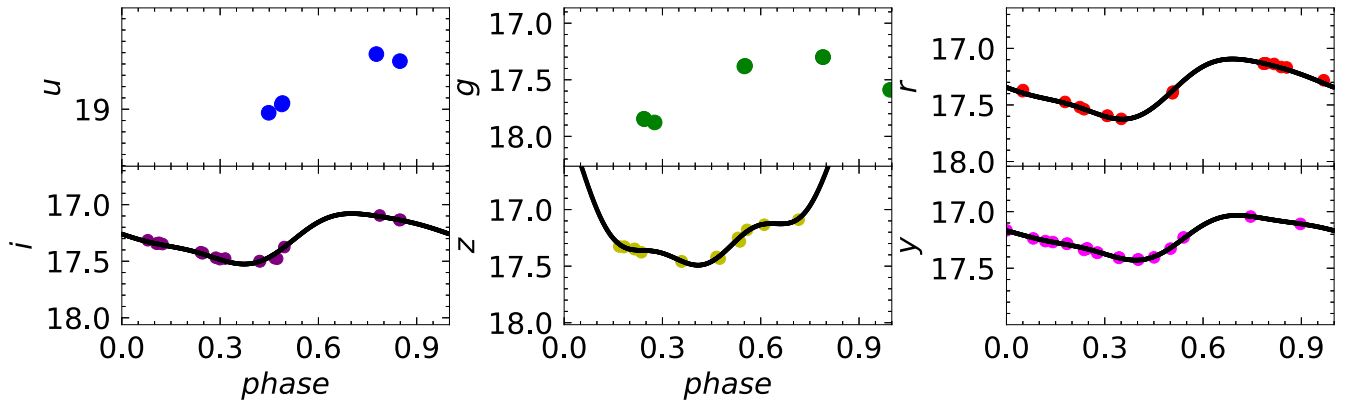


Figure 4. Simulated observations for an RRc in Sagittarius after 1 yr of observations in different magnitude–phase planes (colored filled points). For those photometric bands where `LcFitting` converges (using three harmonics), we have also added the fitting result (black curve). In the z band, our choice of the number of harmonics is clearly too high due to the presence of a large gap in phase.

Table 2
PulsationStarRecovery Output Dictionary

| Name | Description of the output dictionary |
|---------------------------------------|--|
| n_x | No-saturated visits in the X band |
| maxGap_x | Dimension of the largest gaps in phase |
| numberGaps_x | Number of gaps larger than $0.7 \cdot \text{maxGap}_x$ |
| uniformityKS_x | Uniformity measure of the simulated light curve (see Section 2.1 for details) |
| P_{gatspy} | Gatspy best period |
| ΔP_{gatspy} | Absolute value of the difference between Gatspy’s and the model’s period |
| χ_x | Chi of the fitting |
| <code>fittingParametersAllband</code> | A dictionary with all the fitting output ^a |
| $\Delta \text{MeanMag}$ | Difference between the template and fitted LC’s intensity-weighted mean magnitude; |
| ΔAmpl_x | Difference between the template and fitted LC’s peak–peak amplitude. |

^a For all bands zero-point, period, amplitude, and phase of all the harmonics.

In the real case, the matter is more complicated because we have to take into account that the template of pulsating stars oscillates with amplitudes that can be considerably large (see Table 1), and the object is well detected if the observations allow a good recovery of the light curve. Figure 7(a) shows the light curves we expect for the RRab template positioned at the Leo I distance after 10 yr of the survey while Table 5 details the light-curve recovery results. The best recovery of the light curve is obtained in the gri filters, as demonstrated by the lower chi value in the relative photometric bands. In these three filters, as shown in the table, the differences between the measured and the starting (from the model) mean magnitudes and amplitudes are also very small. However, in the remaining bands, the curves are very scattered because the template’s magnitude is close to the detection limit and as a consequence, the fit’s χ and the derived magnitude errors increase. The reduced amplitude increases the effect for the bands close to the infrared (z and y).

Figure 7(b) shows the CEP2-simulated light curve at the Leo I distance. Due to its brighter luminosity, in this case, the light-curve scatter is very limited in all bands, and the fit of the simulated light curve is extraordinarily good (see the black line).

More complicated is the discussion about the recovery of LPVs. As bright stars, they are, in principle, observable up to the

Table 3

Recovered $\Delta \text{MeanMag}$ and ΔAmp in the g and r as a Function of the Number of Observation’s Years for an RRc in Sagittarius Obtained Using Two Harmonics

| Year | n_g | n_r | $\Delta \text{MeanMag}_g$ | $\Delta \text{MeanMag}_r$ | ΔAmp_g | ΔAmp_r |
|------|-------|-------|---------------------------|---------------------------|-----------------------|-----------------------|
| 1 | 8 | 18 | ... | −0.005 | ... | −0.0024 |
| 2 | 19 | 42 | 0.002 | 0.0010 | −0.035 | −0.013 |
| 4 | 28 | 78 | −0.0006 | −0.0002 | −0.064 | −0.028 |
| 6 | 43 | 111 | 0.0041 | −0.0007 | −0.069 | −0.032 |
| 8 | 62 | 147 | 0.009 | −0.0007 | −0.074 | −0.034 |
| 10 | 79 | 181 | −0.001 | 0.002 | −0.045 | −0.016 |

limits of the LG, but having very large amplitudes (6/7 mag in our case) in nearby galaxies (up to Fornax, $d = 0.14$ Mpc), many visits could be saturated, especially in those photometric bands close to the infrared. In Fornax, for example, the percentage of not-saturated visits is 100%, 63%, 54%, 4%, 0.5%, and 0% in the $ugrizy$ filters. We highlight that none of the u visits is saturated, demonstrating the importance of this photometric band for the period and shape recovery of the nearest LPVs.

The situation is even worse if we consider brighter LPVs. This particular scientific case, as all those related to the bright stars of the stellar systems, would benefit from shorter LSST exposures, which is still an open question. On the contrary, due to the large amplitude that characterizes LPVs for the most distant galaxies, a significant part (obviously the less luminous part) of the light curve may fall entirely below the detection limits, making the recovery of the light curve very difficult. For example, Figure 8 shows the light curve in the g band; we expect, after 2 and 10 yr of survey (crosses and filled circles, respectively), for the LPV template to be located at the distance of Sex A, the most distant dwarf of our sample. This plot clearly demonstrates the crucial importance of a 10 yr survey to reconstruct the light curve of this type of LPV. At this point, we recall that a 10 yr baseline will also allow us to search in a systematic way for the possible long second periodicity (LSP) phenomena. Indeed, OGLE’s experience has shown that about 25%–30% of LPVs exhibit long secondary periods, but these variability modes have an unknown origin. It cannot be explained as a fundamental radial pulsation since the long secondary period is typically ~ 4 times longer than the fundamental period. The most favored explanations lean toward binarity and nonradial g modes. However, these and other

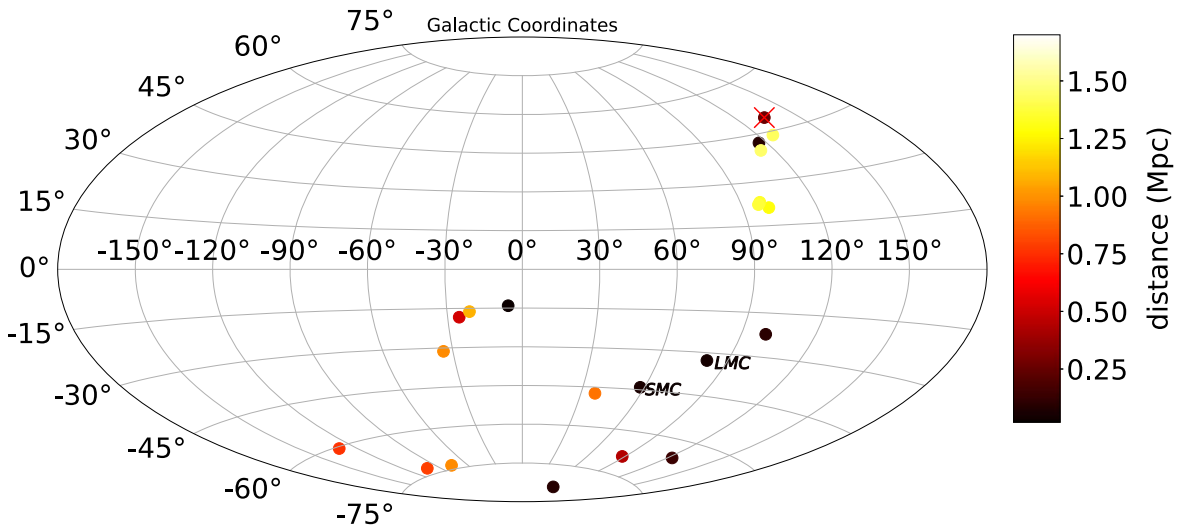


Figure 5. Selected dwarf galaxies in an Aitoff diagram (Galactic coordinates). The location of the Magellanic Clouds is also shown, which will be discussed in detail in Section 3. Leo I is labeled with a red cross (see text).

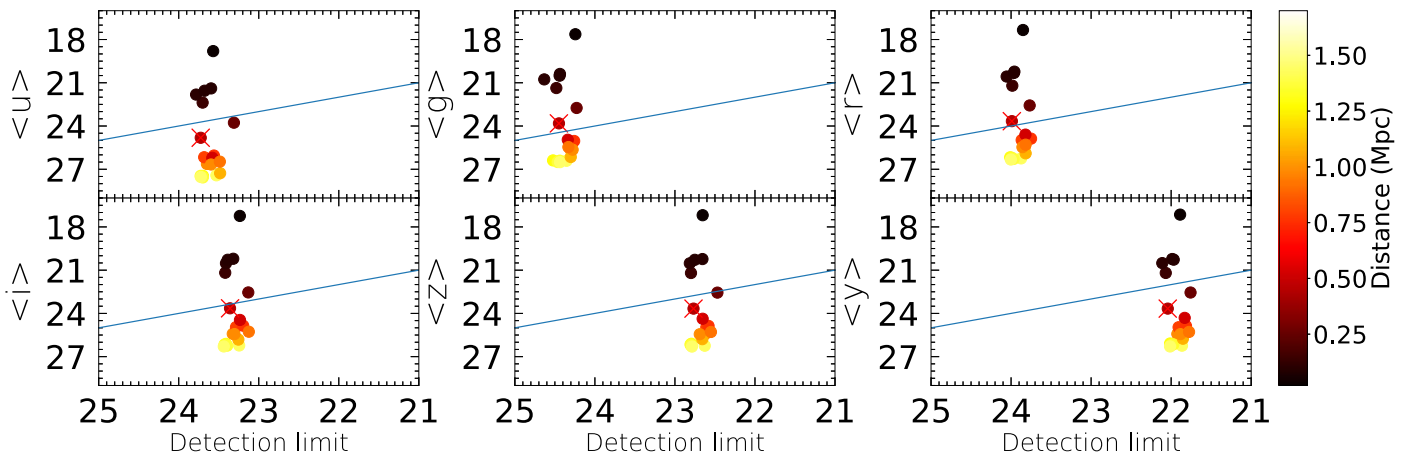


Figure 6. RAB template intensity-weighted mean magnitude at the 3D sky position of selected galaxies of our sample (see Table 4) vs. mean detection limit derived by Opsim at that sky position in different filters. Leo I is marked with a cross (see text).

explanations for LSP all have significant problems (Pawlak 2023) and need more observations to be eventually confirmed.

We stress that the study of the LPVs in environments characterized by different metallicities and ages, such as LG dwarf galaxies, is crucial to understanding the role of LPVs as stellar candles. For example, OGLE and MACHO experiments have shown that LPVs in the MCs form six distinct parallel sequences in the period–luminosity diagram. Wood (2015) and Trabucchi et al. (2019) show that each sequence depends on the pulsation mode responsible for their variability. However, understanding, for example, if one of these relationships can be considered a standard candle is a complex question. In this context, LSST will allow us to perform a study of this object comparable to the OGLE and MACHO ones, with the advantage of extending the analysis to different Galactic and extragalactic environments.

3.1. From *baseline_v2.0_10yrs* to Other Opsim: Changing the Filter Balance

The release of V2.0 survey strategy simulations¹⁷ was recently announced following the SCOC Phase 1.0

¹⁷ All available here: https://github.com/lst-pst/survey_strategy/blob/main/fbs_2.0/SummaryInfo_v2.1.ipynb.

recommendations (see PSTN-053 13).¹⁸ The considerable difference from the previous one is the expansion of the sky area, which receives WFD-like¹⁹ visits and now includes the Galactic Bulge and the Magellanic Clouds, and the addition of a two-region rolling cadence to the majority of the sky. In the previous section, we used *baseline_v2.0_10yrs* as a starting point for our investigation, which is usually considered the reference one. In this section, we will try to understand the significant differences in the light-curve recovery of the considered class of pulsating stars observed when the survey strategy is changed. For this purpose, we have decided to explore those strategies that will have the most profound impact on recovery, keeping in mind the questions asked by the SCOC during the optimization process of the survey strategy.

The primary question we hope to address is if the standard filter balance used in *baseline_v2.0_10yrs* (*u, g, r, i, z, y* are 7%, 9%, 22%, 22%, 20%, and 20% of the total

¹⁸ Actually, at the time of submission of this paper, other Opsims have been released, but they are not particularly interesting for the discussed footprint. These new survey simulations will be taken into consideration in our next paper on the recovery of the light curves of variables in the Galactic Plane.

¹⁹ The Wide–Fast–Deep (WFD) survey will be the main LSST survey that will take between 75% and 85% of the time on sky.

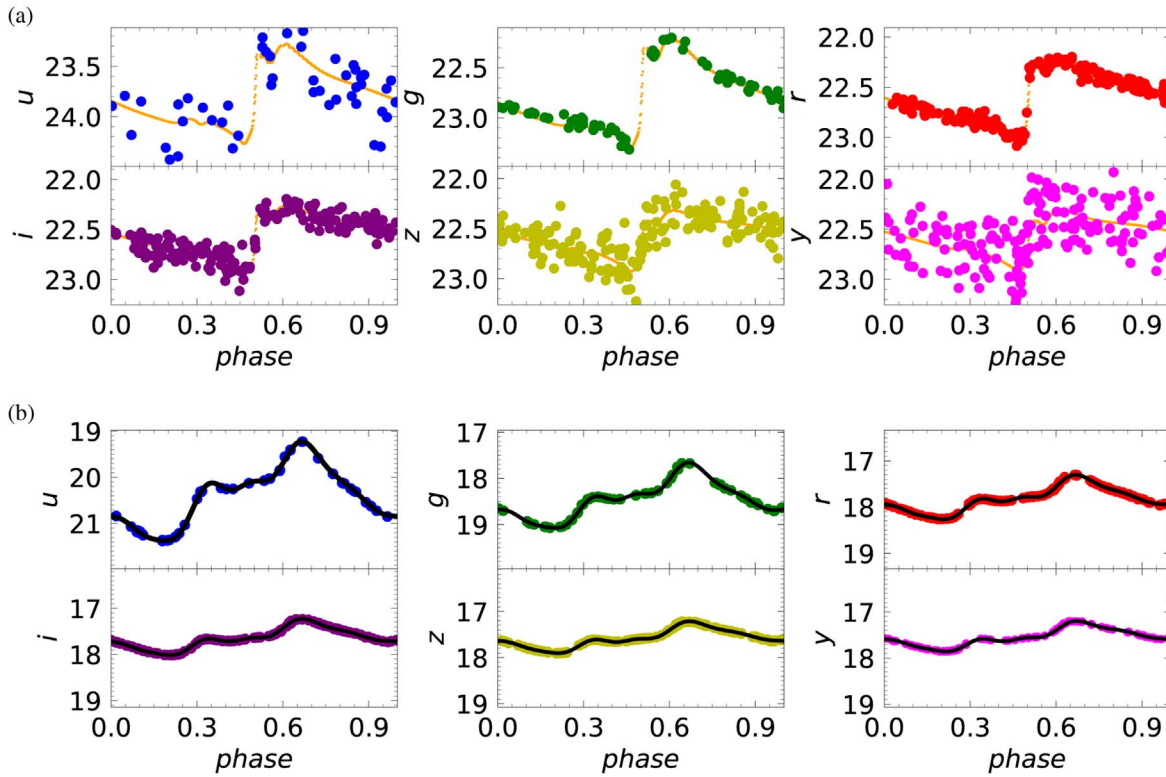


Figure 7. Simulated *ugrizy* light curves of RRab(a) and CEP2(b) in Leo I after 10 yr of observations. The orange curve in (a) is the starting template, while the black line in (b) is the result of the fit performed by `PulsatingStarRecovery` using seven harmonics.

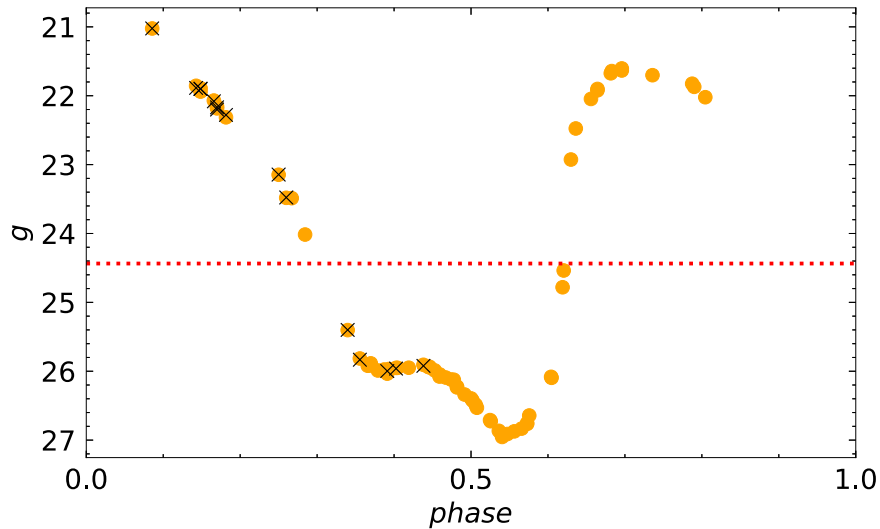


Figure 8. Light curve in the *g* band of LPVs in Sex A after 10 (circle) and 2 (crosses) years. The dotted line represents the detection limit in *g* at the Sex A position in the sky.

number of visits) is appropriate. For our purpose, we would rather have a more significant number of *u* and *g* visits to recover the light curve in all bands simultaneously from the earliest years and to perform a multiwavelength analysis immediately. We have seen in the previous sections that it is impossible to fit the light curve in these two bands in the first year, especially when high harmonics are necessary, as in the case of fundamental-mode RRLs or CCs. The v2.0 release simulations, skewing the filter balance toward blue—as in

bluer_idx0_v2.0_10yrs or *bluer_idx0_v2.0_10yrs*—add very few visits in *u* and *g* (up to 10 visits in *u* and around 20 in *g*, that means just couple of visits each year), which is not enough to produce a better recovery starting from the first year.

Using available rolling cadences such as *rolling_all_sky_ns2_rw0.9_v2.0_10yrs* and *roll_early_v2.0_10yrs*, we do not appreciate significant improvements in recovery parameters derived with `PulsationStarRecovery.py` for all variables considered in this study.

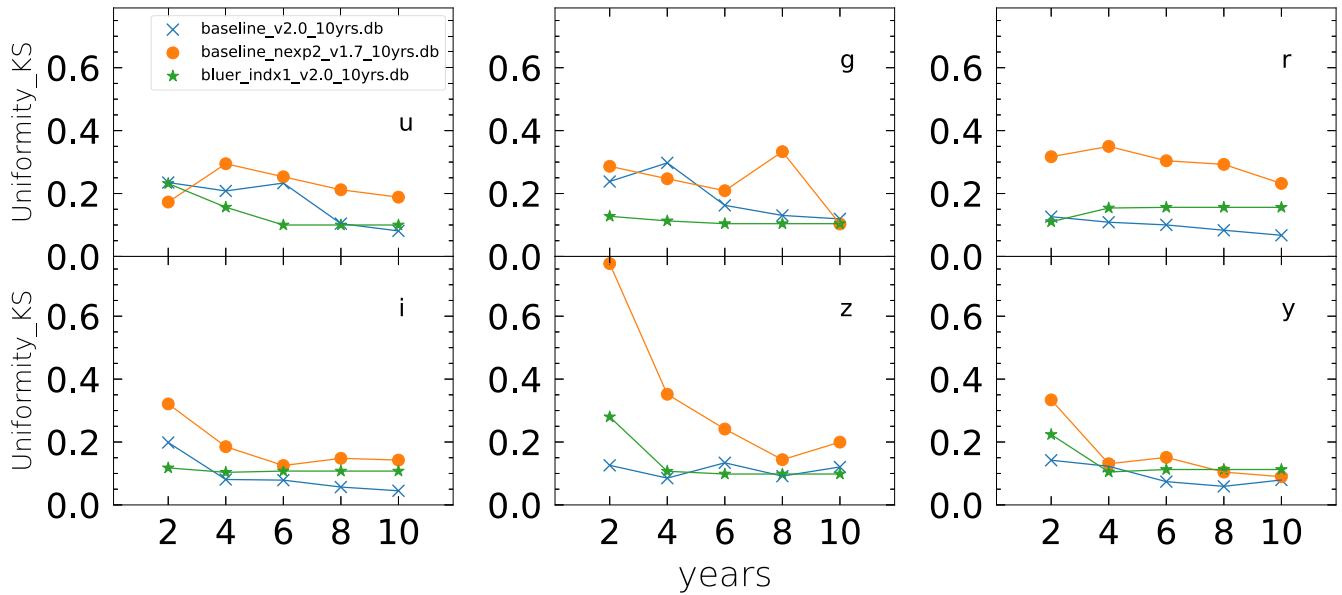


Figure 9. uniformity_{KS_x} in each band and at different survey years for the labeled survey strategies in case of an RRc. We remember that uniformity_{KS} is a value between 0 (uniform sampling) and 1.

Table 4

R.A., Decl. and Distance of Dwarf Galaxies Selected from the Karachentsev et al. (2013) Catalog (See Text)

| n | Name | R.A. | Decl. | Dist. (Mpc) |
|-----|-------------|-----------|-----------|-------------|
| 1 | Sagittarius | 283.7629 | -30.478 | 0.02 |
| 2 | Sculptor | 15.0392 | -33.7092 | 0.09 |
| 3 | Sextans | 153.2625 | -1.6144 | 0.09 |
| 4 | Carina | 100.4029 | -50.9661 | 0.1 |
| 5 | Fornax | 39.9779 | -34.5258 | 0.14 |
| 6 | Leo I | 152.1121 | 12.3081 | 0.26 |
| 7 | Phoenix | 27.7762 | -44.4447 | 0.44 |
| 8 | NGC 6822 | 296.24042 | -14.8030 | 0.52 |
| 9 | IC 1613 | 16.1992 | 2.1333 | 0.76 |
| 10 | Cetus | 6.5458 | -11.0444 | 0.79 |
| 11 | Tucana | 340.4541 | -64.4200 | 0.92 |
| 12 | WLM | 0.4921 | -15.4611 | 0.98 |
| 13 | DDO 210 | 311.7158 | -12.8480 | 0.98 |
| 14 | SagDIG | 292.4958 | -17.6780 | 1.08 |
| 15 | Antlia B | 147.2337 | -25.9900 | 1.29 |
| 16 | NGC 3109 | 150.7800 | -26.16 | 1.34 |
| 17 | Antlia | 151.0167 | -27.3319 | 1.37 |
| 18 | Sex B | 150.0004 | 5.3322 | 1.43 |
| 19 | Sex A | 152.7533 | -4.6928 | 1.45 |
| 20 | LMC | 80.89417 | -69.7561 | 0.05 |
| 21 | SMC | 13.15833 | -72.80028 | 0.06 |

Note. The last two rows give information on MCs that are discussed in more detail in Section 4.

This result was expected since our metric is not sensitive to internight gaps between visits but to the final number of visits.

In conclusion, our final request is to provide more optical visits in the early years, at least for the g band. On the other hand, we have no particular request for how these observations are distributed within one night.

We conclude this section emphasizing that all the Opsim used until now used 2×15 s visits for all bands except the u band, where 1×30 s visits are used to reduce the effects of

readnoise (which are most extreme in u , due to the low sky background). The same simulations exist that extend the u -band visit time further to 1×50 s at the expense of g visits or practically halving the g ones. Since, conversely, we are interested in increasing g visits, we do not support this option. In addition, in the case of the LPVs, longer exposure times for the u band would cause the saturation of a number of visits also in this band, which actually, as shown above, is the only band that allows us to have all nonsaturated visits up to Fornax.

3.2. Minisurvey Family

Since a 10% gain in the effective survey observing time is still hypothetical, the Vera Rubin Observatory’s LSST plan is to utilize the additional observing time for visits for the minisurveys and the Deep Drilling Fields. In SCOC Phase 1 recommendation (PSTN-053) document, all the suggestions that emerged in the WPs and cadence notes were grouped, including the request for deeper g -band imaging in selected local volume galaxies. Furthermore, a family of new Opsims was added to the v2.0 simulations that took these suggestions into account. The SCOC explicitly asked interested researchers to provide feedback on these microsurveys as the phase 2 conclusion approached. Unfortunately, the 10 galaxies selected by SCOC, showing an increase in the g coverage family, are, on average, farther away than ours, and only IC 1613 is in common with our sample.

Since this galaxy is 0.76 Mpc away, RRab and RRc are too weak to hold a good recovery, and CEP1 is at the limit. We have analyzed the effects on the recovery of CEP2’s light curve, adding the minisurvey visits to the visits of the main survey. In Table 6, we show the recovery results after 2 and 10 yr using *local_gal_bindx2_v2.0_10yrs*, which adds a larger number of visits in 10 yr (14, 17, 35, 31, 24, 17, meaning a significant gain of 35% and 21% in u and g , respectively).

The values reported in Table 6 show no significant improvements compared to the results obtained using only WDF visits. Again, we may gain the advantage of optimal

Table 5
Difference between Recovered and Template’s Period (ΔP), Mean Magnitudes ($\Delta \text{MeanMag}$), and Amplitudes (ΔAmp) in All Six Bands Obtained with `PulsatingStarMetryric`’s when RRAb is at the Leo I Distance

| RRab in Leo I | <i>u</i> | <i>g</i> | <i>r</i> | <i>i</i> | <i>z</i> | <i>y</i> |
|---|----------|----------|----------|----------|----------|----------|
| $\Delta \text{MeanMag}$ | 0.015 | 0.014 | −0.006 | 0.012 | 0.020 | −0.008 |
| ΔAmp | 0.125 | −0.017 | 0.033 | 0.028 | 0.045 | 0.018 |
| χ | 0.0015 | 0.0001 | 0.0003 | 0.0003 | 0.0008 | 0.0027 |
| $\Delta P_{\text{gatpsy}} = 1.388\text{e-}05$ | | | | | | |

Note. The last rows show the `LcFitting` χ that is smaller for less-scattered bands (*gri*).

Table 6
Recovered ΔAmp and $\Delta \text{MeanMag}$ in *g* and *r* Filters after 2 (using Three Harmonics) and 10 (using Seven Harmonics) yr of Observation of a CEP2 in IC 1316 with and without the Dedicated Minisurvey Observations as Scheduled in `local_gal_bindx2_v2.0_10yrs`

| Template: CEP2 | <i>u</i> | <i>g</i> | <i>r</i> | <i>i</i> | <i>z</i> | <i>y</i> |
|---|----------|----------|----------|----------|----------|----------|
| WFD | | | | | | |
| $\Delta \text{MeanMag}_{2 \text{ yr}}$ | 0.04 | 0.101 | 0.008 | 0.006 | −0.016 | −0.021 |
| $\Delta \text{MeanMag}_{10 \text{ yr}}$ | −0.024 | −0.004 | −0.004 | −0.003 | −0.001 | 0.001 |
| $\Delta \text{Amp}_{2 \text{ yr}}$ | 0.1730 | −0.238 | 0.0454 | 0.041 | 0.053 | 0.089 |
| $\Delta \text{Amp}_{10 \text{ yr}}$ | 0.011 | 0.015 | −0.007 | −0.013 | −0.010 | −0.019 |
| WFD+minisurvey | | | | | | |
| $\Delta \text{MeanMag}_{2 \text{ yr}}$ | 0.088 | 0.0400 | 0.010 | 0.010 | −0.012 | −0.010 |
| $\Delta \text{MeanMag}_{10 \text{ yr}}$ | 0.003 | −0.003 | −0.003 | −0.0025 | −0.001 | −0.002 |
| $\Delta \text{Amp}_{2 \text{ yr}}$ | 0.101 | −0.086 | 0.039 | 0.027 | 0.042 | 0.063 |
| $\Delta \text{Amp}_{10 \text{ yr}}$ | −0.017 | 0.024 | −0.005 | −0.0105 | −0.013 | −0.023 |

recovery in the first releases and enable early science by adding the extra minisurvey observations in the first 2 yr.

4. Magellanic Clouds

The MCs, the most luminous and largest satellite galaxies of the Milky Way, deserve a separate discussion in this paper. The WFD survey now covers both galaxies, but this has not always been the case. Their presence in the WFD survey is the consequence of the bottom-up process, which, as described in detail in Bianco et al. (2022), has the final aim to maximize the survey science potential while serving as broad a community as possible. During the 2018 LSST Cadence Hackathon, Knut Olsen coordinated a working group composed of members from different SCs (some of them among the authors of this paper) that spent time and resources to show how much physics and discoveries we should have given up by not considering MCs in the main survey (Olsen et al. 2018). This work convinced the SCOC to introduce MCs in the main LSST survey in all the v2.0 Opsim starting from the baseline.

In this section, we use `PulsatingStarRecovery` on different types of pulsating stars at the LMC distance (0.05 Mpc, $E(B - V) = 0.127$) to support this choice.

Figure 9 shows how the RRAb light-curve sampling uniformity changes with survey cadence at different survey stages. The improvement in uniformity moving from `baseline_nexpl_v1.7_10yrs`, which observes MCs only in the South Celestial Pole minisurvey, to `baseline_v2.0_10yrs` is evident. In the same figure, we also show how the uniformity parameter changes using one of the simulations belonging to V2.0 skewing the filter balance toward blue. As expected, improvements in sampling are obtained over the `baseline_v2.0` especially in the *u* bands and *g* bands and in the first years. In Table 7, we show the degree of

Table 7
Light-curve Recovery Parameters Derived from `PulsatingStarRecovery` for Different Types of Templates in the LMC after 10 Yr of Observations

| | RRab | RRc | CEP1 | CEP2 |
|---------------------------|-------------------|----------|---------|----------|
| ΔPeriod | 2.0e-06(0.000989) | 1e-06 | 3e-06 | 0.000301 |
| $\Delta \text{MeanMag}_r$ | 0.0024(0.0522) | −0.0017 | −0.008 | −0.029 |
| $\Delta \text{MeanMag}_g$ | 0.019(0.0156) | −0.00030 | 0.004 | −0.0104 |
| $\Delta \text{MeanMag}_r$ | 0.0005(−0.052) | 7.9e-05 | 0.0007 | −0.0102 |
| $\Delta \text{MeanMag}_i$ | −0.0063(0.015) | 0.0006 | 0.0006 | −4.7e-05 |
| $\Delta \text{MeanMag}_z$ | −0.0013(−0.019) | 0.00016 | −0.0003 | −0.0038 |
| $\Delta \text{MeanMag}_y$ | 0.0025(−0.039) | −0.00057 | 0.0007 | −0.0035 |
| ΔAmp_u | −0.029(0.119) | 0.018 | −0.0129 | −0.0013 |
| ΔAmp_g | −0.049(0.172) | −0.0028 | −0.021 | −0.021 |
| ΔAmp_r | 0.042(0.096) | −0.0034 | −0.032 | −0.032 |
| ΔAmp_i | −0.033(0.129) | −0.0056 | −0.023 | −0.023 |
| ΔAmp_z | −0.040(0.093) | −0.0117 | −0.020 | −0.020 |
| ΔAmp_y | 0.0033(0.0174) | −0.016 | −0.018 | −0.018 |

Note. In brackets, the same values obtained using the South Pole minisurvey visits derived from `baseline_nexpl_v1.7_10yrs`.

accuracy of the recovery of the simulated light curves after 10 yr of LSST observations of different templates of pulsating stars in the LMC with the survey cadence described by `baseline_v2.0_10yrs`. The simulated light curves are shown in Figure 10, with the fit result. Our simulations for RR Lyrae and both Cepheids show excellent recovery results. We obtained an accuracy of the order of thousandths of a magnitude for average magnitudes and hundredths of a magnitude or less for amplitudes in all bands, except for the *u* band for both RR Lyrae, whose light curve is more scattered

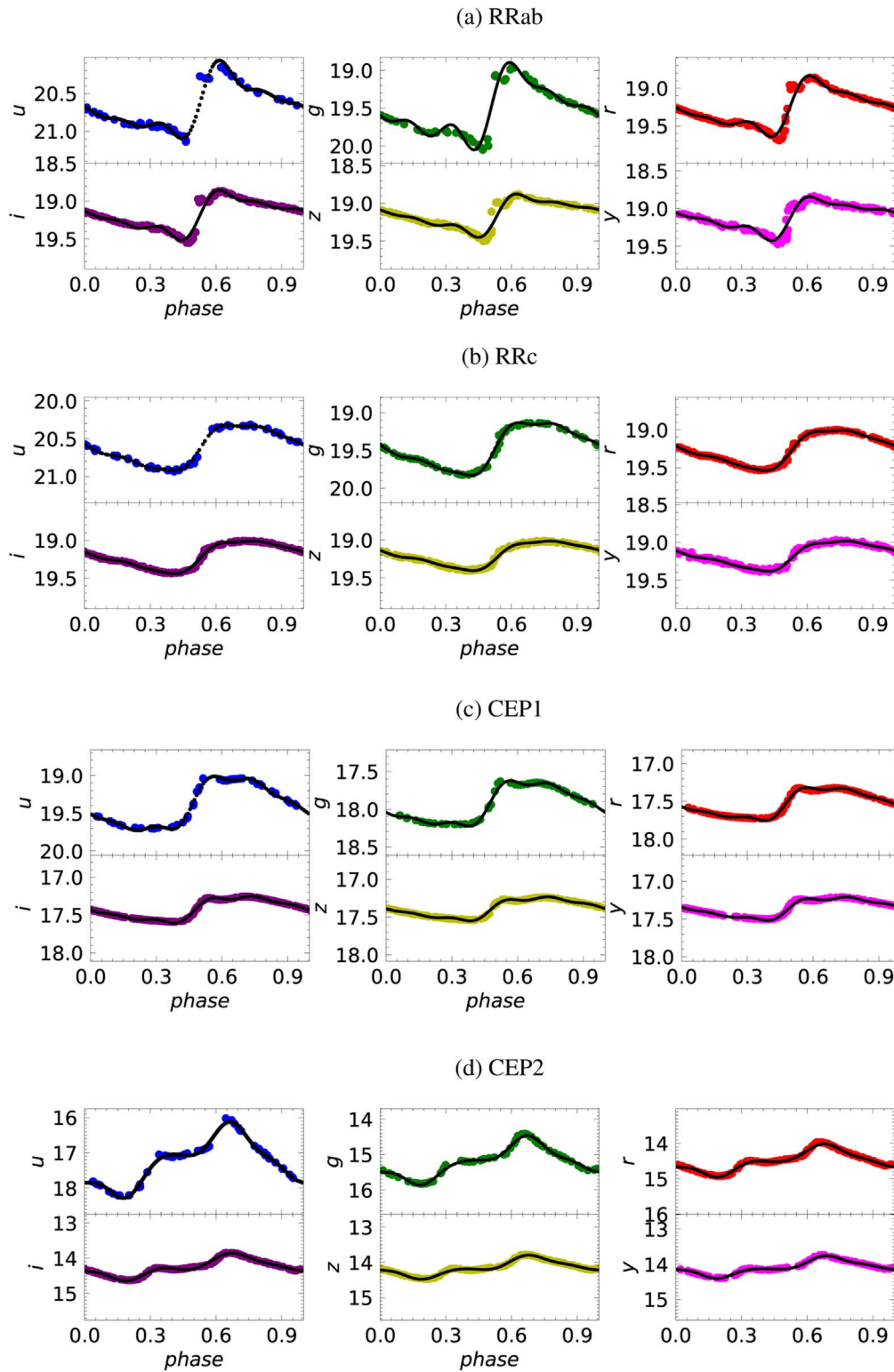


Figure 10. Light-curve fit (with five harmonics) of R Rab (a), R Rc (b), CEP1 (c), and CEP2 (d) in the LMC after 10 yr of observations.

as the derived error magnitude at the LMC distance is large. In parentheses are shown the values obtained using old `baseline_nexp1_v1.7_10yrs`, which observed MCs only in the South Celestial Pole minisurvey: Decreasing the visits from 800 to 250, the light-curve recovery deteriorates after 10 yr, obviously worsening after a couple of years. These

computations support the choice of the SCOC to include the Magellanic Clouds in the main survey.

In the same way, the recovery of the LMC’s LPV light curve could greatly benefit by quadrupling the number of visits. Nevertheless, not all visits will help reconstruct the light curve because many of these will be saturated at the LMC

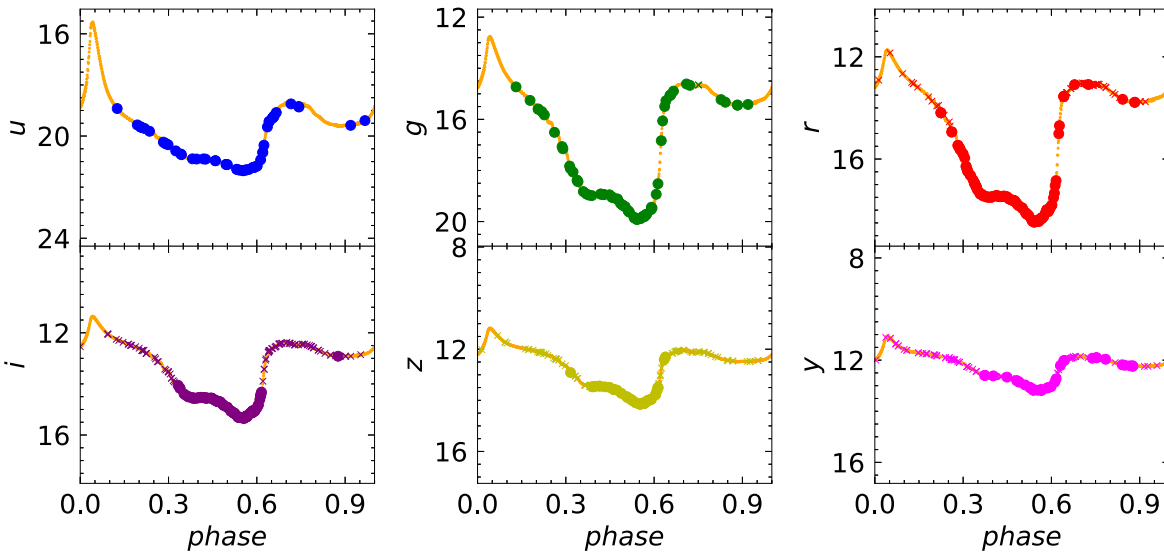


Figure 11. Starting template and simulated LPV light curves in the LMC after 10 yr of LSST observations. Saturated visits are labeled with crosses.

distance due to significant brightness and amplitudes (see Figure 11).

To be more quantitative using our LPV template, only 48%/28%/23% of the izy visits will be under the saturation level defining the good fit of the light curve in these bands. However, almost all ugr visits would be usable for the recovery, at least in the case of the LPVs represented by our template. In any case, there is no better experiment than Rubin LSST to monitor the light curves in six different photometric bands of the LPVs in the MCs and surrounding regions in such a systematic way. Together with the OGLE light curves, Vera Rubin Observatory’s LSST resulting from 10 yr of observations will bequeath an important LPV database in the MCs in the years to come.

5. Conclusions

We have described `PulsatingstarRecovery` as a sophisticated expert metric written within the LSST Survey cadence optimization process to understand the effects of cadence survey strategy on the recovery of the light curve of pulsating stars (RR Lyrae, Cepheids, and LPVs). The metric starts from a template placed at a given position of the 3D sky (that means given R.A., decl., and distance). First, it builds the expected temporal series for a given survey strategy and then analyzes the time series searching for the pulsation period using a multifilter approach. As the last step, our metric computes the best-fit model of the simulated light curve in each photometric band. As a result of this process, the metric gives a few outputs that quantify the LC recovery’s goodness.

Our main effort is to provide the accurate recovery of the light curve in the different photometric bands for three different reasons:

1. The shape of the light curves significantly changes when moving from the u to the y band. Accurate sampling allows us to limit intrinsic errors.
2. Accurate mean magnitudes are useful when using PLZ and PWZ relations to overcome possible systematics.
3. Accurate amplitudes in different photometric bands are key observables, for example, for characterizing the RRL population in the Bailey diagram (Fiorentino et al. 2015, 2017; Monelli & Fiorentino 2022). Moreover,

Fabrizio et al. (2019, 2021), by using metallicity measurements for more than 9000 RRLs, based on either high- or low-resolution spectra, found well-defined and linear relations between period and amplitudes with metallicity for both fundamental and first-overtone RRLs.

4. Together with the amplitudes and the inversion of the PLZ and PWZ relations new calibrations of the Fourier parameters–metallicity relations can be used to provide homogeneous metallicity estimates for field RRLs. In two recent investigations (Mullen et al. 2021, 2022) we provided for the first time new and accurate calibrations of the Fourier parameters–metallicity relations for the optical and MIR bands by using the largest and most homogeneous spectroscopic sample of field RRLs ever collected (Crestani et al. 2021b, 2021a). The same approach can be used for the LSST bands and must be investigated for other types of pulsating stars. This means that accurate sampling on different photometric bands is pivotal for constraining the metallicity distribution of field RRLs. In passing, we note that this approach is independent of uncertainties affecting the individual reddening estimates.

To understand in which LG dwarf galaxies LSST data will allow us to do these things and so much more, we decided to use our metric to study the light-curve recovery of different types of pulsating stars at the positions and distances occupied by a sample of galaxies chosen from the Karachentsev catalog. We have started exploring the latest V2.0 OpSim simulations that feature a survey footprint with an expanded dust-free area and WFD-level visits in the Galactic Bulge and Magellanic Clouds. We naturally started from the “baseline” one. Since the light curves become more and more scattered as the distance increases, mainly in the u , z , and y bands, we showed that a good recovery (at least for optical bands) is possible for the RR Lyrae and the short-period Cepheids up to Leo I at 0.26 Mpc, as demonstrated by fitting parameters reported in Table 3. In particular, we derived an accurate mean magnitude with a precision two orders of magnitude lower than the rms of the theoretical PL and PW relations derived by Marconi et al. (2022). We point out that, when propagating the uncertainties on the PL/PW relations to derive distances, usually the

propagation on the uncertainties of the coefficients is vanishing, while the error on the mean magnitudes and extinction dominate, being at least an order of magnitude larger. Providing such precise mean magnitudes, LSST will allow us to lower the error budget by at least $\sim 40\%$, not taking into account the improvements in extinction estimates.

Concerning early science with Vera Rubin Observatory's LSST, we showed that after the first couple of years, it is already possible to obtain accurate mean magnitudes and periods at least for the most-sampled filters (*rizy*) of RRLs and CCs.

If accurate *u* and *g* mean magnitudes and amplitudes are needed from the beginning of the survey, a different cadence strategy must be adopted. We have demonstrated that the simulations belonging to the V2.0 filter-dist family do not cover this gap. A possible solution could be an early rolling strategy in the *u* and *g* bands to have accurate mean magnitudes and amplitudes or a dedicated minisurvey by the end of the second year of observation. However, we would need more visits than those predicted by available `local_gal_bindx2_v2.0_10yrs.db` for IC 1613, the only dwarf in common with our sample.

Using our template of long-period Cepheids (CEP2) and LPVs, we have also shown that long- and very long-period variables can be recovered excellently up to the LG outskirts. Ten years of the Vera Rubin Observatory's LSST observations will provide the first homogeneous and almost complete census of the LPVs belonging to the LG galaxies. Only in the case of large-amplitude LPVs (such as the one represented by our template) do we expect saturation problems for LPVs at a distance closer than Fornax (including those in the MCs) or otherwise problems with detection near the minimum for more distant ones. LSST data will clarify our pulsation and dust formation models, enabling us to understand how the pulsation period amplitudes and modes relate to properties such as stellar mass, luminosity, and mass at different metallicities and NIR excess.

These studies are crucial to understanding the role of LPVs as distance indicators, which is still a debated question.





Finally, we have shown how our metric allows us to support the SCOC's decision to include MCs in the main survey showing that we will obtain excellent recovery of the light curves of all types of pulsating variables crucial for making impact science in the coming years.

We are already working on the second paper of this series, where we will use `PulsatingStarRecovery` in a different Galactic environment that will significantly benefit from LSST observations from the point of view of pulsating variables: the Galactic Plane. In that paper, we will describe a new function that we are integrating into our metric that can show the effect of the blend from nearby stars on the recovery of the light curve. Needless to say, this extension of the metric will also be essential in understanding what happens in the central areas of the most crowded dwarf that we have considered.

We are grateful to the SCOC and to the TVS and SMWLVRubin SCs for the support given during the last months during the Cadence Strategy Optimization. This work was supported by the Preparing for Astrophysics with the LSST Program,

funded by the Heising-Simons Foundation through grant 2021-2975, and administered by Las Cumbres Observatory. In particular, M.D.C., S.L., and V.B. were supported by the "Period and shape recovery of light curves of pulsating stars in different Galactic environments (KSI-8)" and K.C. and Y.C. by the "Building a Diverse Generation of Rubin Scientists (KSP-8)" grant. This work is dedicated to the late Antonio Sollima, colleague and friend, who left us too soon.

ORCID iDs

M. Di Criscienzo  <https://orcid.org/0000-0003-4132-1209>
 V. Braga  <https://orcid.org/0000-0001-7511-2830>
 I. Musella  <https://orcid.org/0000-0001-5909-6615>
 G. Bono  <https://orcid.org/0000-0002-4896-8841>
 M. Dall'Ora  <https://orcid.org/0000-0001-8209-0449>
 G. Fiorentino  <https://orcid.org/0000-0003-0376-6928>
 M. Marconi  <https://orcid.org/0000-0002-1330-2927>
 R. Molinaro  <https://orcid.org/0000-0003-3055-6002>
 V. Ripepi  <https://orcid.org/0000-0003-1801-426X>
 K. Carrell  <https://orcid.org/0000-0002-6307-992X>

References

- Bailey, S. I. 1902, *AnHar*, **38**, 1
 Bianco, F. B., Ivezić, Z., & Jones, R. 2022, *ApJS*, **258**, 1
 Cacciari, C., et al. 2005, *AJ*, **129**, 267
 Chen, Y., Girardi, L., Fu, X., et al. 2019, *A&A*, **632**, A105
 Clementini, G., Musella, I., Chieffi, A., et al. 2018, arXiv:1812.03298
 Crestani, J., Braga, V. F., Fabrizio, M., et al. 2021a, *ApJ*, **914**, 10
 Crestani, J., Fabrizio, M., Braga, V. F., et al. 2021b, *ApJ*, **908**, 20
 De Somma, G., Marconi, M., Molinaro, R., et al. 2020, *ApJS*, **247**, 30
 Delgado, F., & Reuter, M. A. 2016, *Proc. SPIE*, **9910**, 991013
 Fabrizio, M., Bono, G., Braga, V. F., et al. 2019, *ApJ*, **882**, 169
 Fabrizio, M., Braga, V. F., Crestani, J., et al. 2021, *ApJ*, **919**, 118
 Fiorentino, G., Bono, G., Monelli, M., et al. 2015, *ApJL*, **798**, L12
 Fiorentino, G., Monelli, M., Stetson, P. B., et al. 2017, *A&A*, **599**, A125
 Hambleton, K. M., Bianco, F. B., Street, R., et al. 2022, arXiv:2208.04499
 Ivezić, Z., Kahn, S. M., Tyson, J. A., et al. 2019, *ApJ*, **873**, 111
 Jones, R. L., et al. 2020, Survey Strategy and Cadence Choices for the Vera C. Rubin Observatory Legacy Survey of Space and Time (LSST), v1.2
 Zenodo, doi:10.5281/zenodo.4048838
 Jursic, J., & Kovacs, G. 1996, *A&A*, **312**, 111
 Karachentsev, I. D., Makarov, D. I., & Kaisina, E. I. 2013, *AJ*, **145**, 101
 Marconi, M., Coppola, G., Bono, G., et al. 2015, *ApJ*, **808**, 50
 Marconi, M., Molinaro, R., Dall'Ora, M., et al. 2022, *ApJ*, **934**, 29
 Monelli, M., & Fiorentino, G. 2022, *Univ*, **8**, 191
 Mullen, J. P., Marengo, M., Martínez-Vázquez, C. E., et al. 2021, *ApJ*, **912**, 144
 Mullen, J. P., Marengo, M., Martínez-Vázquez, C. E., et al. 2022, *ApJ*, **931**, 131
 Musella, I., Di Criscienzo, M., Braga, V., et al. 2021, Classical Variable Stars in Different Galactic Environments: Pulsation Behaviour Recovery, Cadence Note, https://docushare.lsst.org/docushare/dsweb/Get/Document-37629/Pulsating_stars.pdf
 Nemeč, et al. 2013, *ApJ*, **773**, 181
 Olsen, K., Di Criscienzo, M., Jones, R. L., et al. 2018, arXiv:1812.03139
 Pawlak, M. 2023, *A&A*, **669**, A60
 Reuter 2016, *Proc. SPIE*, **9911**, 991125
 Simon, & Lee 1981, *ApJ*, **248**, 291
 Trabucchi, M., Wood, P. R., Montalbán, J., et al. 2019, *MNRAS*, **482**, 929
 Trabucchi, M., Wood, P. R., Mowlavi, N., et al. 2021, *MNRAS*, **500**, 1575
 Vanderplas, J. 2015, gatspy: General tools for Astronomical Time Series in Python v0.1.1, Zenodo doi:10.5281/zenodo.14833
 VanderPlas, J. T., & Ivezić, Z. 2015, *ApJ*, **812**, 18
 Wood, P. R. 2015, *MNRAS*, **448**, 3829